DESIGN OF ALKALI ACTIVATED SLAG–FLY ASH CONCRETE MIXES USING MACHINE LEARNING

Chamila Gunasekera, Weena Lokuge, Medina Keskic, Nawin Raj, David W. Law, Sujeeva Setunge

Biography: Chamila Gunasekara is a Postdoctoral Research Fellow in the School of Engineering, RMIT University, Australia. His research interests include advanced construction materials & characterization, and performance of alkali activated materials and geopolymers.

Weena Lokuge is a Senior Lecturer in School of Civil Engineering and Surveying, University of Southern Queensland, Australia. Her research interests include Green construction materials-Polymer concrete, alkali activated concrete and durability of FRP composites.

Medina Keskic is a graduate engineer from School of Engineering, RMIT University, Australia. Her research interests include performance of different concretes, including alkali activated materials, geopolymers and high volume fly ash concretes.

Nawin Raj is a Lecturer in School of Agricultural, Computational and Environmental Sciences, University of Southern Queensland, Australia. His research interests are applied mathematics, nonlinear dynamics and theoretical and computational fluid dynamics.

David W. Law is a Senior Lecturer in the School of Engineering, RMIT University. His research interests are investigating sustainable materials and material properties of concrete, performance of reinforced concrete structures and alkali activated/geopolymer concretes.

Sujeeva Setunge is a Professor and Deputy Dean of School of Engineering at RMIT University. Her research interests include concrete technology, alkali activated/geopolymer concrete, and Infrastructure management and disaster resilience.

ABSTRACT

So far, the alkali activated concrete has primarily focused on the effect of source material properties and ratio of mix proportions on the compressive strength development. A little research has focused on developing a standard mix design procedure for alkali activated concrete for a range of compressive strength grades. This study developed a standard mix design procedure for alkali activated slag–fly ash (low calcium, class F) blended concrete using two machine learning techniques, Artificial Neural Networks (ANN) and Multivariate Adaptive Regression Spline (MARS). The algorithm for the predictive model for concrete mix design was developed using MATLAB programming environment by considering the five key input parameters; water/solid ratio, alkaline activator/binder ratio, Na-Silicate /NaOH ratio, fly ash/slag ratio and NaOH molarity. The targeted compressive strengths ranging from 25–45 MPa (3.63–6.53 ksi) at 28 days were achieved with laboratory testing, using the proposed machine learning mix design procedure. Thus, this tool has the capability to provide a novel approach for the design of slag-fly ash blended alkali activated concrete grades matching to the requirements of in-situ field constructions.

Key-words: Alkali Activated Concrete; Artificial Neural Networks; Multivariate Adaptive Regression Spline model; Mix design; Compressive strength

INTRODUCTION

Portland cement (PC) is one of the most manmade consumable materials worldwide and its current annual production exceeded 4.2 billion metric tonnes [1, 2]. The speedy surge in consumption and demand, the large greenhouse gases emissions and the high production cost of PC have encouraged the need of developing sustainable alternative construction binders. The cement production itself is responsible for 5–7% of total carbon dioxide emissions worldwide [3]. Thus, it is an urgent essentiality for alternative, sustainable cementitious materials, which can decrease the dependence on PC in construction. Alkali activated concrete can be produced using blended industrial waste of fly ash and blast furnace slag, which can reduce carbon dioxide emissions by 25–45% [4]. The blended slag–fly ash reacts with concentrated alkaline activator and form three-dimensional aluminosilicate cross-linked network. The blended alkali activated concrete is gaining importance as it is getting applied in the actual in situ field construction projects in Australia and many other countries [2].

The use of alkali activated concrete in specific applications requires a carefully designed mix with required characteristics such that the structural members will perform as required throughout the design life. However, the mix design process for alkali activated concrete is complex due to the varying chemical and physical properties of fly ash and slag. Literature has shown that the properties of source materials and the alkali activated concrete mix design directly influence the final properties of blended alkali activated concrete [5-7]. Optimization by artificial intelligence tools has used been for mix design of PC concrete: for instance, the genetic algorithm [8, 9] and particle swarm optimization algorithm [10, 11] were applied to evaluate engineering properties of PC concrete mixtures.

To date, few studies have been conducted to develop a unique mix design procedure using artificial neural networks, which can in turn predict the compressive strength of the alkali activated concrete produced utilizing different binding materials [12, 13]. Nazari Torgal [12] developed six different artificial neural network models while changing number of neurons in hidden layers and model finalizing methods and predicted the compressive strength of different types of alkali activated concrete. They have considered seven independent input parameters such as curing time, calcium hydroxide content, superplasticizer content, NaOH concentration, mould type, alkali activated concrete type and water to sodium oxide molar ratio. The authors [12] concluded that the use of artificial neural networks to predict the compressive strength of different alkali activated concrete mixes was able to be done in a relatively short span of time with minimal error rates. Topcu and Saridemir [14] also used artificial neural networks along with fuzzy logic and observed that the compressive strength development of alkali activated concrete with different binding materials can be predicted through the use of artificial neural networks in a short period of time with minimal error in comparison to the experimentally results. Bondar [13] concluded that the optimum network architecture to predict compressive strength of alkali activated concrete was one with a three-layer feed forward network with tan-sigmoid function as the hidden layer transfer function and a linear function as the output layer.

Lahoti et al. [15] investigated the effect of Si/Al molar ratio, water/solids ratio, Al/Na molar ratio and H_2O/Na_2O molar ratio in determining the compressive strength of metakaolin based alkali activated concrete. The machine learning-based classifiers were engaged for the strength predictions and the results illustrated that Si/Al ratio is the most significant parameter followed by Al/Na ratio. Machine learning-based classifiers were able to predict the compressive strength with high precision. Nazari and Sanjayan [16] further worked with support vector machine technique to predict compressive strength of alkali activated concretes. Due to the complexity of models, the support vector machine parameters were found using five different optimization algorithms including genetic algorithm, particle swarm optimization algorithm, ant colony optimization algorithm, artificial bee colony optimization algorithm and imperialist competitive algorithm. The authors [16] concluded that hybrid models can be appropriately used for modelling of compressive strength of alkali activated paste, mortar and concrete specimens.

Despite the in-depth research carried out in the field of alkali activated concrete and proposed different methods to calculate mix proportions, the development of a suitable mix design procedure for this novel concrete is still in the experimental stage: almost all the proposed methods using different techniques are mainly dependent on the trial and error approach [17, 18]. In this study, five key factors, water/solid ratio, alkaline activator/binder ratio, Na-Silicate /NaOH ratio, fly ash/slag ratio and NaOH molarity have been identified for the compressive strength development. Based on the parameters, a new standard mix design procedure for alkali activated slag–fly ash (low calcium, class F) blended concrete has been developed and the effectiveness of predicting the compressive strength was tested using ANN and MARS models.

SIGNIFICANCE OF RESEARCH

To date alkali activated concrete has primarily focused on the effect of source material properties and ratio of mix proportions on the compressive strength development. Little research has focused on developing a standard mix design procedure for alkali activated slag–fly ash blended concrete for a range of compressive strength grades. This study evaluates the development of a standard mix design procedure for this alkali activated concrete using two machine learning techniques and determines the most reliable statistical model to calculate the mix proportions for a targeted range of compressive strengths of alkali activated slag–fly ash blended concrete. Overall, the proposed methodology demonstrated an effective engineering strategy that can be applied in problems of structural and construction engineering prospective.

MIX DESIGN DATABASE

An inclusive literature review was conducted to establish a database for mix designs of alkali activated slag–fly ash (low calcium, class F) blended concrete based on 28-day compressive strength. Before the application of the machine learning models to the database, data pre-processing was conducted to remove the outliers. Database consists of compressive strength values obtained from 208 concrete mix designs, reported in 45 journal publications, **Table 1**.

Table 1

MACHINE LEARNING MODELS

Data Pre-processing

The accuracy of statistical or machine learning modelling depends upon the accuracy and reliability of data. Outliers are mostly defined as data points which are a minority that have patterns quite different to the majority of other data points in the sample [56]. Any presence of outliers in the data will significantly affect how the machine learning models will effectively train the model for forecasting [57, 58]. **Table 2** shows the statistics for both input variables (water/solid ratio, alkaline activator/binder ratio, Na-Silicate /NaOH ratio, fly ash/slag ratio and NaOH molarity) and the output (i.e. compressive strength) considered in the model development. The low values of skewness and kurtosis for water/solid, NaOH molarity and compressive strength are an indication of the asymmetry about the mean values and they are light tailed too.

Table 2

In this paper, the methods of Hampel [59] and Cook's distance [60] are used to detect and remove the outliers to improve the dataset for machine learning modelling. The raw dataset in this study was tested using both the methods and all samples were carefully screened as rows before the data points were excluded. This is an iterative and tedious process with the nine input samples. The presence of an outlier in one sample could remove valuable data in other sample sets, thus the occurrence of outliers across rows of data were checked to ensure that there are more than two outliers in each row to have it excluded prior to the modelling process. However, in any sample, if the outlier had a significant deviation from the core of the data, that particular outlier was removed. Hampel method computes the median (m_e) for a data set and then calculates the deviation (a_i) from the median value. Each data point (e_i) is subjected to this calculation: $a_i = (e_i - m_e)$, where, i belongs to a set of n (number of data points). If the condition, $|a_i| \geq 4.5(me_{|a_i|})$ is satisfied, then the value is accepted as an outlier. Fig.1 shows an example of 2 input variables with the original data and the refined data when the outliers are removed.

Fig. 1

The Cook's method of removing outliers is mostly used to detect the influence of data points in a regression analysis [61]. Cook's distance D_i of observation k is given in **Eq. 1**:

$$D_i = \frac{\sum_{i=1}^{n}(\hat{y}_i - (\hat{y}_{i(k)})^2}{pMSE} \tag{1}$$

Where, $\hat{y}_i$ is the ith fitted response value, $\hat{y}_{i(k)}$ is the ith fitted response value when the fit excludes observation k, MSE is the mean squared error, p is the number of coefficients in the regression model. **Fig. 2** shows the scatter plots of outliers detected by Cook's method in two of the input samples. This was applied to the entire dataset. Moreover, the boxplots in Fig. 3 show the data distribution in the raw and refined dataset. It is evident from the figure that the majority of the outliers are related to the input parameters, Activator/Binder ratio and Na_2SiO_3/NaOH ratio.

Fig. 2 & Fig. 3

Artificial Neural Networks

Recent studies have relied on the use of Artificial Neural Networks (ANN) to help predict compressive strength of GPC with different binding materials [13, 62]. In recent years, ANN has been used in the civil engineering industry to overcome many problems such as determining structural damage, the modelling of material behaviour, and ground water monitoring [14]. ANNs are described as a series of parallel architectures that work cooperatively to solve complex problems by connecting simple computing elements [62]. The networks utilise learning capabilities obtained from example inputs, which make them perfect for use in the prediction of GPC compressive strength as available data is fairly limited. An artificial neuron contains five main parts: inputs, weights, sum function, activation function and outputs [14]. The inputs are the known data collected from previous test results. Weights are values that demonstrate the effect that the input values have on the outputs. The effect of the weights is calculated by the sum function. The weighted sums of inputs are calculated by **Eq. 2**:

$$(net)_j = \sum_{i=1}^{n} w_{ij}\, x_i + b \qquad (2)$$

Where, $(net)_j$ is the weighted sum of the j^{th} neuron for the input received from the preceding layer with n neurons, w_{ij} is the weight between the j^{th} neuron in the preceding layer, x_i is the output of the i^{th} neuron in the preceding layer, b is a fixed value as internal addition and Σrepresents the sum function [14]. The activation function is one which processes the net input obtained through the sum function and defines the output values. The output is created using a sigmoid function as given in **Eq. 3**:

$$(out)_j = f(net)_j = \frac{1}{1 + e^{-\alpha (net)_j}} \qquad (3)$$

Where, α is a constant used to control the slope of the semi-linear region [14]. Topcu and Saridemir [14] used ANNs along with fuzzy logic to predict the strength development of GPC with different binding materials. They found that compressive strengths can be predicted through the use of ANNs in a short period of time with minimal error in comparison to test results. Bondar [63] concluded that the optimum network architecture to predict compressive strength of GPC was one with a three-layer feed forward network with tan-sigmoid function as the hidden layer transfer function and a linear function as the output layer. Nazari et al. [13, 62] similarly concluded that the use of ANNs to predict the compressive strength of different GPC mixes was able to be done in a relatively short span of time with minimal error rates. They utilised a two-layer feed forward-back propagating network. It was decided to use a three-layer feed forward network with a tan-sigmoid function as the hidden layer function, similar to that by Bondar [63], in this study to predict the mix design of a alkali activated concrete with 32 MPa (4.64 ksi) compressive strength.

Multivariate Adaptive Regression Splines (MARS) model

The MARS model was originally proposed by Friedman [64]. It is a form of a stepwise linear regression and suitable for higher dimensional inputs. In the reported literature the MARS model appears to be more popular than its counterparts such as Artificial Neural Networks and Extreme Learning Machine [65] because of its adaptively synthesized model structure compared to the fixed model structures of its counterparts. MARS predictive modelling has been widely used in hydro-meteorological analysis, most recently in predicting the evaporation loss [66, 67], and in predicting the behaviour of fibre reinforced polymer confined concrete [68].

In MARS algorithm, training data sets are divided into separate piecewise linear segments (splines) of different gradients (slopes). These splines are connected together smoothly, and the piecewise curves are known as basis functions (BFs) producing a model able to handle linear as well as nonlinear behaviour. The connection points are called knots. Between any two knots, MARS characterises data either globally or using linear regression. $BF(x)$ is the basis function for the x intersects at the knot. Let Y be the target dependent variable and $X = (x_1, x_2 \ldots\ldots x_p)$ be the input independent variables. For a continuous response, the relationship between Y and X can be expressed using the MARS model as $Y = f(x_1, x_2 \ldots \ldots \ldots \ldots .. x_p) + e = f(X) + e$: Where e is the fitting error and $f(X)$ is the MARS model with the BFs. For simplicity for this research, only piecewise linear functions are considered. In the MARS environment, the following expression, **Eq. 4**, can be used to predict compressive strength of fly ash based alkali activated concrete (Y).

$$Y = c_0 + \sum_{n=1}^{N} c_m \, BF(x) \tag{4}$$

x is the input variable, c_0 is a constant and c_m is the coefficient of $BF(x)$. During the construction of MARS model, the basis functions are selected based on the generalized cross validation (GCV) in **Eq. 5**.

$$GCV(N) = \left(\frac{1}{n} \frac{\sum_{m=1}^{N} (y_i - \hat{y}_i)^2}{\left(1 - \frac{C(M)}{n}\right)^2} \right) \tag{5}$$

n is the number of data points, y_i is the actual value of data point i, $\hat{y}_i$ is the predicted value for data point i and $C(M)$ is the penalty factor defined as $C(M) = M + dM$: where d is the cost penalty factor of each basis function optimisation. When several basis functions are selected in the forward phase, over-fitting can occur. Therefore, deleting some basis functions in the backward phase is important to select the optimised model.

MARS and ANN model development

The algorithm for the predictive model for alkali activated concrete mix design was developed using MATLAB programming environment. In order to develop the MARS model, the database shown in **Table 2** was analysed to establish the key mix design parameters. These were identified as the fly ash/slag ratio, water/solid ratio, activator/binder ratio, Na-Silicate /NaOH ratio and NaOH molarity as predictive variables. When developing the MARS and ANN predictive models, it is important to select a training data subset and a testing subset to evaluate the model performance. The portioning of the available database between the training and testing subsets was decided based on each application and there is no fixed approach for this division. In the literature, it is reported that 63-80% of the available data has been used for the training [65, 69-71]. In a more recent study, 60% of the data was selected for training, the 20% selected for testing while the remaining was selected for validation [65]. It was decided in this study to select 68 of the available data (~70%) for the training and use the remainder as the testing subset. A random sampling process was used in partitioning the database into training and testing to achieve optimum results. The randomly sampled data set was used in the development and training stage of the model while the testing dataset was used in the model verification stage. As the initial stage of the model development, all the input and output data sets were normalized to get a range between 0 and 1 using:

$x_{normalised} = \frac{(x - x_{minimum})}{(x_{maximum} - x_{minimum})}$; where, x is any data point (input or output), $x_{normalised}$ is the normalized value of the data set, $x_{minimum}$ is the minimum value of the set of data and $x_{maximum}$ is the highest value of the same data set. In the MARS model construction, 19 basis functions were used in the forward phase and 6 of them were deleted in the backward phase leaving 13 basis functions in the final optimum MARS model. ANN model architecture consists of 8 input parameters, with 10 neurons in the hidden layer leading to only one target which is the compressive strength. **Fig. 4**

MARS and ANN model evaluation

Once the predictive model is developed, it is important to test the model by using the actual and predicted compressive strengths of alkali activated concrete. The performance of the

MARS model developed was evaluated using coefficient of correlation (R), mean square error (RMSE) and mean absolute error (MAE) [65], **Eq. 6.1–6.3**.

$$R = \frac{\sum_{i=1}^{n}(Y_{ai} - \bar{Y_a})(Y_{pi} - \bar{Y_p})}{\sqrt{\sum_{i=1}^{n}(Y_{ai} - \bar{Y_a})^2}\sqrt{\sum_{i=1}^{n}(Y_{pi} - \bar{Y_p})^2}} \quad (6.1)$$

$$RMSE = \sqrt{\frac{\sum_{i=1}^{n}(Y_{ai} - Y_{pi})^2}{n}} \quad (6.2)$$

$$MAE = \frac{\sum_{i=1}^{n}|Y_{ai} - Y_{pi}|}{n} \quad (6.3)$$

Where, Y_{ai} and Y_{pi} are actual and predicted compressive strengths, $\bar{Y_a}$ and $\bar{Y_p}$ are the mean of the actual and predicted values while n is the number of data samples. The performance indicators of the MARS model for the training and testing data sets are shown in **Table 3**. The training data set is having a better correlation with the actual values. It is evident that ANN performed better than MARS, the values of R, RMSE and MAE show that ANN predicted values estimate the actual compressive strength values quite well. **Fig. 5** shows the scatter plots of the ANN model and MARS models.

Table 3 & Fig. 5

The histogram of absolute prediction error of the ANN and MARS models are shown in **Fig. 6.** Most of the errors are clustered towards zero indicating a good performance of the models in forecasting the compressive strength based on the training of the input samples. **Fig. 7** shows the comparison of actual compressive strength with ANN and MARS simulated values. Both methods make good predictions of the compressive strength with the exception of few points.

Fig. 6 & Fig. 7

DESIGN OF ALKALI ACTIVATED CONCRETE

Contour Plots

Four different contour plots obtained from analytical model are illustrated in **Fig. 8**. The compressive strength of alkali activated concrete is dependent on all the five variables that have been identified, and these contour maps can be used to design mix proportions achieving required compressive strengths at 28 days. Fig. 8(a) shows that when water/solid ratio varies between 0.15 and 0.3, and activator/binder ratio increases, the compressive strength is increased. However, when water/solid ratio increase beyond 0.3, the compressive strength started to decrease with increasing the activator/binder ratio. Higher compressive strength can also be achieved with a higher water/solid ratio, but also with lower activator/bind ratio and lower fly ash/slag ratio, Fig. 8(a/d). Fig. 8(b) shows that a combination of a higher activator/binder ratio and a lower Na-Silicate /NaOH ratio will yield a higher compressive strength. For a range of Na-Silicate /NaOH of 1.0 to 4.5, a range of compressive strengths can be achieved (25–45 MPa / 3.63–6.53 ksi) if the activator/binder ratio is between 0.55 and 0.75. In contrast, Fig. 8(c) shows that either lower activator/binder ratio combined with a lower NaOH molarity or higher activator/binder ratio combined with a higher NaOH molarity can result in higher compressive strengths. That is, when activator/binder ratio varies from 0.35-0.55 and NaOH molarity differs from 7-10 or activator/binder ratio varies from 0.55-0.75 and NaOH molarity differs from 10-14, the range of compressive strengths between 25 and 45 MPa (3.63 and 6.53 ksi) can be achieved.

Fig. 8

Mix design calculation

In order to validate the model developed using machine learning, four concrete mixes were designed with the targeted compressive strength of 25 MPa (3.63 ksi), 30 MPa (4.35 ksi), 40 MPa (5.80 ksi) and 45 MPa (6.53 ksi). For instance, in the 30 MPa (4.35 ksi) concrete mix, the five mix design variables obtained from contours shown in Fig. 8 were: water/solid ratio, activator/binder ratio, Na-Silicate /NaOH ratio, fly ash/slag ratio and NaOH molarity were 0.33, 0.70, 3.2, 6.0 and 10.5, respectively. The majority of the alkali activated slag–fly ash blended concrete mixes in Table 1 used a total binder content (i.e. fly ash and slag) of 400-420 kg (882-926 lb). The total binder content in the mix designs used for this study is taken as 410 kg (904 lb), a median value of the reported range. The volume percentage of coarse aggregate/total aggregate in concrete generally varies between 0.60 and 0.75 [72]. For this study, the $V_{Aggregate}/(V_{Sand} + V_{Aggregate})$ ratio is taken as 0.65.

(a) Calculate fly ash and slag content:

$$fly\ ash + slag = 410 \text{ and } \frac{fly\ ash}{\text{slag}} = 6.0$$

After solving: Fly ash = 351.4 kg (774.7 lb) and Slag = 58.6 kg (129.2 lb)

(b) Calculate alkaline activator content:

$$\frac{Activator}{Binder} = \frac{\text{Na}_2\text{SiO}_3 + \text{NaOH}}{Total\ Binder} = 0.7 \text{ and } \frac{\text{Na}_2\text{SiO}_3}{\text{NaOH}} = 3.2$$

After solving: Na-Silicate = 218.7 kg (482.2 lb) and NaOH = 68.3 kg (150.6 lb)

(c) Calculate required added water content:

$$\frac{Water}{Solid} = \frac{\text{Na}_2\text{SiO}_{3_{water}} + \text{NaOH}_{water} + \text{Added Water}}{Binder + \text{Na}_2\text{SiO}_{3_{solid}} + \text{NaOH}_{solid}} = 0.33$$

	Na-Silicate	NaOH	Added water	Binder	Total
Solid	96.4	19.8	0	410	526.2
Water	122.3	48.5	w	0	170.8 + w

After solving: Added water (w) = 2.85 kg (6.28 lb).

It was noted that the alkali activation process releases water during the dissolution of the species and formation of aluminosilicate gel [73]. As such, water plays the role of a reaction medium, but resides within pores in the gel. In order to maintain the workability, extra water will be added to the concrete mix as required.

(d) Calculate fine and coarse aggregate content:

The fine and coarse aggregate content in alkali activated concrete mix is calculated based on the absolute volume (V) method [72]. It is noted that the PC concrete in the fresh mix stage can entrain entrapped air upto 2% by volume [72]. For simplicity, this factor is not included in the calculations .

$$V_{Fly\ ash} + V_{\mathrm{Na_2SiO_3}} + V_{NaOH} + V_{Added\ water} + V_{Sand} + V_{Aggregate} = 1$$

$$\frac{M_{Fly\ ash}}{\rho_{Fly\ ash}} + \frac{M_{\mathrm{Na_2SiO_3}}}{\rho_{\mathrm{Na_2SiO_3}}} + \frac{M_{NaOH}}{\rho_{NaOH}} + \frac{M_{Added\ water}}{\rho_{Added\ water}} + \frac{M_{Sand}}{\rho_{Sand}} + \frac{M_{Aggregate}}{\rho_{Aggregate}} = 1$$

$$\frac{V_{Aggregate}}{V_{Sand} + V_{Aggregate}} = 0.65$$

where ρ is specific material density (kg/m^3).

After solving: M_{Sand} = 538.6 kg (1187.4 lb) and $M_{Aggregate}$ = 1042.5 kg (2298.3 lb)

Similarly, the mix proportions of specific blended alkali activated concrete was calculated and tabulated in **Table 4**.

Table 4

Experimental Procedure

The alkali activated slag-fly ash blended concrete was produced using Class F low calcium fly ash, obtained from Gladstone power plant in Australia and commercially available blast furnace slag. The X-ray fluorescence analysis, X-ray diffraction analysis and Malvern particle size (Mastersizer X) analysis were conducted to examine the chemical composition, mineralogical composition and particle size distribution of raw materials, respectively. The surface area of fly ash and slag were determined using Brunauer Emmett Teller (BET) method by N_2 absorption.

Table 5 & Table 6

The liquid sodium hydroxide and liquid Na-Silicate (Na_2O=14.7% and SiO_2=29.4% by mass, specific gravity=1.53) were used as alkaline activator in the alkali activated concrete production. The fine aggregate and coarse aggregate were prepared with respect to the Australian Standards, AS 1141.5 [74]. River sand in uncrushed form (specific gravity=2.5 and fineness modulus= 2.8) was used as fine aggregate, and 10mm grain size crushed granite aggregate (specific gravity=2.65 and water absorption=0.74%) was used as coarse aggregate in concrete. Demineralized water was used throughout in the mixing.

The fly ash-slag binder, river sand and coarse aggregate were mixed using a 60 litre concrete mixer for 4 minutes. Next Na-Silicate, sodium hydroxide and water were added and mixed continuously for another 8 minutes in order to obtain a glossy and well combined concrete mix. The alkali activated concrete mix was poured into 100x100x100 mm cubic Teflon moulds, and then vibrated using a vibration table for 1 minute to remove air bubbles. Finally, the concrete moulds were kept at laboratory conditions (23°C/73.4°F temperature and 70% relative humidity) for 24 hours. Next concrete moulds were removed, and specimens were cured in water until being tested at 7 and 28 days. The 7-day and 28-day compressive strengths of alkali activated concrete were tested using a MTS machine with a loading rate of 20 MPa/min (2.9 ksi/min) in accordance with AS 1012.9 standard [75].

Experimental results and Model validation

The compressive strength development of four slag-fly ash blended concrete mixes, i.e. 25 MPa (3.63 ksi), 30 MPa (4.35 ksi), 40 MPa (5.80 ksi) and 45 MPa (6.53 ksi), between 7 and 28 days are displayed in **Fig. 9**. The experimental data confirmed that four alkali activated concrete mixes achieved their specific targeted compressive strength or very closer to the required compressive strength at 28 days. Only the M25 mix displayed a little reduction compared to the desired compressive strength. All alkali activated concrete s achieved strength increase between 7 and 28 days, but in different percentage. The M25 mix obtained the highest strength development (43%) while M40 gained the lowest strength increase (19.3%) during this period. Overall, test results showed a good correlation between the targeted and achieved compressive strength of slag-fly ash blended concrete by following the proposed mix design method using machine learning techniques. The current model has identified five key mix design parameters and can be applied to design concrete grades ranging from 25 to 45 MPa (3.63 to 6.53 ksi).

Literature [6, 76-78] indicates that a number of inter related factors influence the compressive strength of the alkali activated/geopolymer concrete. The particle size distribution together with the specific surface area, and the reactive amorphous percentage of source materials (i.e. fly ash and blast furnace slag) are the governing parameters of compressive strength development [79-82]. In addition, the commercially available Na-Silicate solution has many chemical species, such as monomer, dimer, trimer, cyclic, polymeric, rings etc., whose relative contents are dependent upon the SiO_2/Na_2O molar ratio. These varieties of chemical species can be expected to influence the alkali activation of source materials, which in turn affect the compressive strength development [83, 84]. Overall, it is recommended that including these factors in mix design procedure at future study would further increase the accuracy and reliability of this model to use in filed applications with more confidence.

Fig. 9

SUMMARY AND CONCLUSIONS

An extensive literature review was conducted in order to obtain the mix design details and corresponding compressive strengths of alkali activated slag–fly ash (low calcium) blended concrete. Two machine learning approaches, Artificial Neural Networks (ANN) and Multivariate Adaptive Regression Spline (MARS) techniques have been utilised to develop this model in order to design the alkali activated concrete mixes with a target compressive strength at 28 days. The main contribution from this study is the use of model created using machine learning techniques to develop contour plots to present the relationship between the five key parameters, namely water/solid ratio, alkaline activator/binder ratio, Na-Silicate /NaOH ratio, fly ash/slag ratio and NaOH molarity that influence the compressive strength of blended concrete. The algorithm for the predictive model for alkali activated concrete mix design was developed using MATLAB programming environment. A detailed calculation for a 30 MPa (4.35 ksi) alkali activated concrete mix design is presented in order to demonstrate the use of these contour plots to design concrete mix proportions. Correspondingly, the four alkali activated concrete mixes were designed, and an experimental program was conducted to measure the actual compressive strength. The test results, ranging from 25 MPa to 45 MPa (3.63 to 6.53 ksi), are in good agreement with the predicted compressive strengths from the contour plots, hence validating the model. As such, the proposed contour plots together with the methodology can be used to develop mix designs for alkali activated slag-fly ash (Class F, low calcium) blended concrete.

ACKNOWLEDGEMENT

The authors wish to acknowledge Flyash Australia Pty Ltd. and Cement Australia Pty Ltd. for the supply of low calcium fly ash and blast furnace slag for the research. The X-ray facility and Microscopy & Microanalysis facility provided by RMIT University with the scientific and technical assistance is also acknowledged. This research was conducted by the Australian Research Council Industrial Transformation Research Hub for nanoscience based construction material manufacturing (IH150100006) and funded by the Australian Government.

REFERENCES

1. countries, G.c.p.t. 2017, Statistic, Statista. (n.d.).
2. Australia, C.C.A. 2016; Available from: Available from: http://www.concrete.net.au/iMIS_Prod.
3. Mathew, G. and Joseph, B. Flexural behaviour of geopolymer concrete beams exposed to elevated temperatures. Journal of Building Engineering 2018. 15: p. 311-317.
4. Turner, L.K. and Collins, F.G. Carbon dioxide equivalent (CO2-e) emissions: A comparison between geopolymer and OPC cement concrete. Construction and Building Materials 2013. 43(1): p. 125-130.
5. Wardhono, A., Gunasekara, C., Law, D.W., and Setunge, S. Comparison of long term performance between alkali activated slag and fly ash geopolymer concretes. Construction and Building materials 2017. 143: p. 272-279.
6. Gunasekara, C., Law, D.W., Setunge, S., and Sanjayan, J.G. Zeta potential, gel formation and compressive strength of low calcium fly ash geopolymers. Construction and Building Materials 2015. 95(1): p. 592-599.
7. Diaz-Loya, E., Allouche, E.N., and Vaidya, S. Mechanical properties of fly-ash-based geopolymer concrete. ACI Materials Journal 2011. 108(3): p. 300-306.
8. Lim, C.-H., Yoon, Y.-S., and Kim, J.-H. Genetic algorithm in mix proportioning of high-performance concrete. Cement and Concrete Research 2004. 34(3): p. 409-420.
9. Camp, C.V., Pezeshk, S., and Hansson, H. Flexural design of reinforced concrete frames using a genetic algorithm. Journal of Structural Engineering 2003. 129(1): p. 105-115.
10. Gilan, S.S., Jovein, H.B., and Ramezanianpour, A.A. Hybrid support vector regression–particle swarm optimization for prediction of compressive strength and RCPT of concretes containing metakaolin. Construction and Building Materials 2012. 34: p. 321-329.

11. Cheng, R., Pomianowski, M., Wang, X., Heiselberg, P., and Zhang, Y. A new method to determine thermophysical properties of PCM-concrete brick. Applied energy 2013. 112: p. 988-998.

12. Nazari, A. and Torgal, F.P. Predicting compressive strength of different geopolymers by artificial neural networks. Ceramics International 2013. 39(3): p. 2247-2257.

13. Bondar, D. The Use of Artifical Neural Networks to Predict Compressive Strength of Geopolymers. 2011.

14. Topcu, I.B. and Sarıdemir, M. Prediction of compressive strength of concrete containing fly ash using artificial neural networks and fuzzy logic. Computational Materials Science 2008. 41(3): p. 305-311.

15. Lahoti, M., Narang, P., Tan, K.H., and Yang, E.-H. Mix design factors and strength prediction of metakaolin-based geopolymer. Ceramics International 2017. 43(14): p. 11433-11441.

16. Nazari, A. and Sanjayan, J.G. Modelling of compressive strength of geopolymer paste, mortar and concrete by optimized support vector machine. Ceramics International 2015. 41(9, Part B): p. 12164-12177.

17. Ferdous, W., Manalo, A., Khennane, A., and Kayali, O. Geopolymer concrete-filled pultruded composite beams–Concrete mix design and application. Cement and Concrete Composites 2015. 58: p. 1-13.

18. Anuradha, R., Sreevidya, V., Venkatasubramani, R., and Rangan, B.V. Modified guidelines for geopolymer concrete mix design using Indian standard. Asian Journal of civil engineering (Building and Housing) 2012. 13(3): p. 353-64.

19. Khan, M. and Castel, A. Effect of MgO and Na2SiO3 on the carbonation resistance of alkali activated slag concrete. Magazine of Concrete Research 2017. 70(13): p. 685-692.

20. Rajamane, N., Nataraja, M., Dattatreya, J., Lakshmanan, N., and Sabitha, D. Sulphate resistance and eco-friendliness of geopolymer concretes. Indian Concrete Journal 2012. 86(1): p. 13.
21. Prashanth, P., Lakshmi, M.P., and Manohar, G. EXPERIMENTAL STUDY ON GEOPOLYMER CONCRETE. International Journal of Creative Research Thoughts (IJCRT) 2018. 6(1): p. 309-312-309-312.
22. Nuccetelli, C., Trevisi, R., Ignjatović, I., and Dragaš, J. Alkali-activated concrete with Serbian fly ash and its radiological impact. Journal of environmental radioactivity 2017. 168: p. 30-37.
23. Kumar, S.S., Pazhani, K., and Ravisankar, K. Fracture behaviour of fibre reinforced geopolymer concrete. Current Science (00113891) 2017. 113(1).
24. Chitrala, S., Jadaprolu, G.J., and Chundupalli, S. Study and predicting the stress-strain characteristics of geopolymer concrete under compression. Case studies in construction materials 2018. 8: p. 172-192.
25. Sreenivasulu, C., Ramakrishnaiah, A., and Jawahar, J.G. Mechanical properties of geopolymer concrete using granite slurry as sand replacement. International Journal of Advances in Engineering & Technology 2015. 8(2): p. 83.
26. Sreenivasulu, C., GURU, J.J., SEKHAR, R.M.V., and PAVAN, K.D. Effect of fine aggregate blending on short-term mechanical properties of geopolymer concrete. 2016.
27. Jawahar, J.G. and Mounika, G. Strength properties of fly ash and GGBS based geo polymer concrete. Asian Journal of Civil Engineering (BHRC) 2016. 17(1): p. 127-135.
28. Abhilash, P., Sashidhar, C., and Reddy, I.R. Strength properties of Fly ash and GGBS based Geo-polymer Concrete. International Journal of ChemTech Research, ISSN 2016: p. 0974-4290.

29. Sreenivasulu, C., Jawahar, J.G., and Sashidhar, C. Predicting compressive strength of geopolymer concrete using NDT techniques. Asian Journal of Civil Engineering 2018. 19(4): p. 513-525.
30. Pavani, P., Roopa, A., Jawahar, J.G., and Sreenivasulu, C. INVESTIGATION ON GEOPOLYMER CONCRETE USING GRANITE SLURRY POWDER AS PARTIAL REPLACMENT OF FINE AGGREGATE. 2016.
31. VenkataKiran, P., Jawahar, J.G., Sashidhar, C., and Sreenivasulu, C. Flexural Studies on Fly Ash and GGBS Blended Reinforced Geopolymer Concrete Beams.
32. Ren, J.-r., Chen, H.-g., Sun, T., Song, H., and Wang, M.-s. Flexural behaviour of combined FA/GGBFS geopolymer concrete beams after exposure to elevated temperatures. Advances in Materials Science and Engineering 2017. 2017.
33. Palankar, N., Ravi Shankar, A., and Mithun, B. Investigations on Alkali-Activated Slag/Fly Ash Concrete with steel slag coarse aggregate for pavement structures. International Journal of Pavement Engineering 2017. 18(6): p. 500-512.
34. Farhan, N.A., Sheikh, M.N., and Hadi, M.N. Engineering Properties of Ambient Cured Alkali-Activated Fly Ash–Slag Concrete Reinforced with Different Types of Steel Fiber. Journal of Materials in Civil Engineering 2018. 30(7): p. 04018142.
35. Farhan, N.A., Sheikh, M.N., and Hadi, M.N. Experimental investigation on the effect of corrosion on the bond between reinforcing steel bars and fibre reinforced geopolymer concrete. in Structures. 2018; Elsevier.
36. Sashidhar, C., GURU, J.J., Neelima, C., and PAVAN, K.D. Preliminary Studies on self compacting geopolymer concrete using manufactured sand. 2016.
37. Karthik, A., Sudalaimani, K., and Kumar, C.V. Investigation on mechanical properties of fly ash-ground granulated blast furnace slag based self curing bio-geopolymer concrete. Construction and Building Materials 2017. 149: p. 338-349.

38. Ronad, A., Karikatti, V., and Dyavanal, S. A study on mechanical properties of geopolymer concrete reinforced with basalt fiber. International Journal of Research in Engineering and Technology (IJRET) 2016. 5(7): p. 474-478.

39. Krishnaraja, A., Sathishkumar, N., Kumar, T.S., and Kumar, P.D. Mechanical behaviour of geopolymer concrete under ambient curing. International Journal of Scientific Engineering and Technology 2014. 3(2): p. 130-132.

40. Rafeet, A., Vinai, R., Soutsos, M., and Sha, W. Guidelines for mix proportioning of fly ash/GGBS based alkali activated concretes. Construction and Building Materials 2017. 147: p. 130-142.

41. Valencia-Saavedra, W., de Gutiérrez, R.M., and Gordillo, M. Geopolymeric concretes based on fly ash with high unburned content. Construction and Building Materials 2018. 165: p. 697-706.

42. Valencia Saavedra, W.G., Angulo, D.E., and Mejia de Gutierrez, R. Fly ash slag geopolymer concrete: Resistance to sodium and magnesium sulfate attack. Journal of Materials in Civil Engineering 2016. 28(12): p. 04016148.

43. Saavedra, W.G.V. and de Gutiérrez, R.M. Performance of geopolymer concrete composed of fly ash after exposure to elevated temperatures. Construction and Building Materials 2017. 154: p. 229-235.

44. Junaid, M.T. Properties of ambient cured blended alkali activated cement concrete. in IOP Conference Series: Materials Science and Engineering. 2017; IOP Publishing.

45. Singh, B., Rahman, M., Paswan, R., and Bhattacharyya, S. Effect of activator concentration on the strength, ITZ and drying shrinkage of fly ash/slag geopolymer concrete. Construction and Building Materials 2016. 118: p. 171-179.

46. Nath, P. and Sarker, P.K. Fracture properties of GGBFS-blended fly ash geopolymer concrete cured in ambient temperature. Materials and Structures 2017. 50(1): p. 32.

47. Nath, P. and Sarker, P.K. Flexural strength and elastic modulus of ambient-cured blended low-calcium fly ash geopolymer concrete. Construction and Building Materials 2017. 130: p. 22-31.

48. Deb, P.S., Nath, P., and Sarker, P.K. The Effects of GGBFS blending with Flyash and activator content on the workability and strength properties of Geopolymer concrete cured at ambient temperature. Material & design 2014. 62: p. 32-39.

49. Fang, G., Ho, W.K., Tu, W., and Zhang, M. Workability and mechanical properties of alkali-activated fly ash-slag concrete cured at ambient temperature. Construction and Building Materials 2018. 172: p. 476-487.

50. Deb, P., Nath, P., and Sarker, P. Properties of fly ash and slag blended geopolymer concrete cured at ambient temperature. New Developments in Structural Engineering and Construction 2013: p. 571-576.

51. Deb, P., Nath, P., and Sarker, P. Sulphate Resistance of Slag Blended Fly Ash Based Geopolymer Concrete. in Concrete 2013: Proceedings of the 26th Biennial National Conference of the Concrete Institute of Australia. 2013; Concrete Institute of Australia.

52. Vignesh, P. and Vivek, K. An experimental investigation on strength parameters of flyash based geopolymer concrete with GGBS. International Research Journal of Engineering and Technology (IRJET) 2015. 2(02).

53. Pandurangan, K., Thennavan, M., and Muthadhi, A. Studies on Effect of Source of Flyash on the Bond Strength of Geopolymer Concrete. Materials Today: Proceedings 2018. 5(5): p. 12725-12733.

54. Ushaa, T., Anuradha, R., and Venkatasubramani, G. Performance of self-compacting geopolymer concrete containing different mineral admixtures. 2015.

55. Ramineni, K., Boppana, N.K., and Ramineni, M. Performance Studies on Self-Compacting Geopolymer Concrete at Ambient Curing Condition. in International Congress on Polymers in Concrete. 2018; Springer.

56. Hadi, A.S., Imon, A.R., and Werner, M. Detection of outliers. Wiley Interdisciplinary Reviews: Computational Statistics 2009. 1(1): p. 57-70.

57. Li, W., Mo, W., Zhang, X., Squiers, J.J., Lu, Y., Sellke, E.W., Fan, W., DiMaio, J.M., and Thatcher, J.E. Outlier detection and removal improves accuracy of machine learning approach to multispectral burn diagnostic imaging. Journal of Biomedical Optics 2015. 20(12): p. 1-9, 9.

58. Baskar, S., Arockiam, L., and Charles, S. A systematic approach on data pre-processing in data mining. Compusoft 2013. 2(11): p. 335.

59. Hampel, F.R. A General Qualitative Definition of Robustness. The Annals of Mathematical Statistics 1971. 42(6): p. 1887-1896.

60. Cook, R.D. Detection of Influential Observation in Linear Regression. Technometrics 1977. 19(1): p. 15-18.

61. Jagadeeswari, T., Harini, N., Satya Kumar, C., and Tech, M. Identification of outliers by cook's distance in agriculture datasets. Int. J. Eng. Comput. Sci 2013. 2: p. 2319-7242.

62. Nazari, A., Khalaj, G., Riahi, S., Bohlooli, H., and Kaykha, M.M. Prediction total specific pore volume of geopolymers produced from waste ashes by ANFIS. Ceramics International 2012. 38(4): p. 3111-3120.

63. Bondar, D. Use of a Neural Network to Predict Strength and Optimum Compositions of Natural Alumina-Silica-Based Geopolymers. Journal of Materials in Civil Engineering 2013. 26(3): p. 499-503.

64. Friedman, J.H. Multivariate adaptive regression splines. The annals of statistics 1991: p. 1-67.

65. Deo, R.C., Samui, P., and Kim, D. Estimation of monthly evaporative loss using relevance vector machine, extreme learning machine and multivariate adaptive regression spline models. Stochastic environmental research and risk assessment 2016. 30(6): p. 1769-1784.

66. Samui, P. Slope stability analysis using multivariate adaptive regression spline. Metaheuristics Water Geotech Transp Eng 2012. 14: p. 327.

67. Adamowski, J., Fung Chan, H., Prasher, S.O., Ozga-Zielinski, B., and Sliusarieva, A. Comparison of multiple linear and nonlinear regression, autoregressive integrated moving average, artificial neural network, and wavelet artificial neural network methods for urban water demand forecasting in Montreal, Canada. Water Resources Research 2012. 48(1).

68. Mansouri, I., Ozbakkaloglu, T., Kisi, O., and Xie, T. Predicting behavior of FRP-confined concrete using neuro fuzzy, neural network, multivariate adaptive regression splines and M5 model tree techniques. Materials and Structures 2016. 49(10): p. 4319-4334.

69. Boadu, F.K. Rock properties and seismic attenuation: neural network analysis. Pure and Applied Geophysics 1997. 149(3): p. 507-524.

70. Kurup, P.U. and Dudani, N.K. Neural networks for profiling stress history of clays from PCPT data. Journal of Geotechnical and Geoenvironmental Engineering 2002. 128(7): p. 569-579.

71. Samui, P. and Dixon, B. Application of support vector machine and relevance vector machine to determine evaporative losses in reservoirs. Hydrological Processes 2012. 26(9): p. 1361-1369.

72. Neville, A.M., Properties of Concrete. Fourth and Final Edition ed. Standards updated to 2002. 1996, Harlow: Pearson Education Limited.

73. Duxson, P., Fernández-Jiménez, A., Provis, J., Lukey, G., Palomo, A., and van Deventer, J. Geopolymer technology: the current state of the art. Journal of Materials Science 2007. 42: p. 2917-2933.

74. AS, Methods for sampling and testing aggregates, Method 5: Particle density and water absorption of fine aggregate, in AS (Australian Standards). 2000, Standards Australia: Australia. p. 1-8.

75. AS, Method of testing concrete, Method 9: Determination of the compressive strength of concrete specimens, in AS (Australian Standards). 1999, Standards Australia: Australia. p. 1-12.

76. Gunasekara, C., Law, D.W., Setunge, S., Burgar, I., and Brkljaca, R. Effect of Element Distribution on Strength in Fly Ash Geopolymers. ACI Materials Journal 2017. 144(5).

77. Diaz-Loya, E.I., Allouche, E.N., and Vaidya, S. Mechanical properties of fly-ash-based geopolymer concrete. ACI materials journal 2011. 108(3): p. 300.

78. Chindaprasirt, P., Chareerat, T., Hatanaka, S., and Cao, T. High-strength geopolymer using fine high-calcium fly ash. Journal of Materials in Civil Engineering 2011. 23(3): p. 264-270.

79. Provis, J.L. Geopolymers and other alkali activated materials: why, how, and what? . Materials and Structures 2014. 47(1-2): p. 11-25.

80. Provis, J.L. and van Deventer, J.S.J. Geopolymerisation kinetics. 1. In situ energy-dispersive X-ray diffractometry. Chemical engineering science 2007. 62(9): p. 2309-2317.

81. Duxson, P., Provis, J.L., Lukey, G.C., and van Deventer, J.S.J. The role of inorganic polymer technology in the development of 'green concrete'. Cement and Concrete Research 2007. 37(12): p. 1590-1597.

82. Dirgantara, R., Gunasekara, C., Law, D.W., and Molyneaux, T.K. Suitability of Brown Coal Fly Ash for Geopolymer Production. Journal of Materials in Civil Engineering 2017. 29(12): p. 04017247.

83. Cho, Y.-K., Yoo, S.-W., Jung, S.-H., Lee, K.-M., and Kwon, S.-J. Effect of Na2O content, SiO2/Na2O molar ratio, and curing conditions on the compressive strength of FA-based geopolymer. Construction and Building Materials 2017. 145: p. 253-260.

84. Gao, K., Lin, K.-L., Wang, D., Hwang, C.-L., Shiu, H.-S., Chang, Y.-M., and Cheng, T.-W. Effects SiO2/Na2O molar ratio on mechanical properties and the microstructure of nano-SiO2 metakaolin-based geopolymers. Construction and building materials 2014. 53: p. 503-510.

TABLES

List of Tables:

Table 1 – Mix design database

Slag (kg)	Fly ash (kg)	Aggregates (kg)		Activator (kg)		Added Water (kg)	Solid % (Na-Silicate)		NaOH solution		Compressive Strength (MPa)	Refer.
		Coarse	Fine	NaOH	Na-Silicate		SiO_2	Na_2O	Molarity	Density (g/cm^3)		
240	80	1215	715	46	114	80	29.4	14.7	12M	1.37	35.5	[19]
240	80	1215	715	46	114	80	29.4	14.7	12M	1.37	47.7	
340	85	1065	390	164	0	58	29.4	14.7	12M	1.37	37.0	
340	85	1065	390	82	82	67	29.4	14.7	12M	1.37	56.0	
223	95	1160	753	61	75	85	25.5	12.8	10M	1.32	64.3	
228	98	1160	753	63	77	79	25.5	12.8	10M	1.32	64.3	
230	99	1145	742	63	77	87	25.5	12.8	10M	1.32	64.3	
300	100	1068	712	12	74	133	29.5	11.5	10M	1.32	52.1	
236	101	1145	742	65	79	82	25.5	12.8	10M	1.32	64.3	
307	102	1293	554	41	102	55	29.4	13.7	10M	1.32	55.5	
307	102	1293	554	41	102	55	29.4	14.7	10M	1.32	55.5	
240	103	1160	753	66	81	68	25.5	12.8	10M	1.32	64.3	
245	105	1111	721	68	82	93	25.5	12.8	10M	1.32	64.3	
319	106	1152	636	10	65	136	32.8	14.7	10M	1.32	55.6	
248	106	1145	742	68	83	70	25.5	12.8	10M	1.32	64.3	
319	106	1152	636	10	65	136	32.8	14.7	10M	1.32	56.2	
319	106	1063	638	23	47	164	16.5	33.0	10M	1.32	51.0	[20]
319	106	1063	638	67	168	0	16.5	33.0	10M	1.32	51.0	
319	106	1155	628	10	65	136	32.8	14.7	10M	1.32	55.4	
251	108	1111	721	69	84	87	25.5	12.8	10M	1.32	64.3	
264	113	1111	721	73	89	75	25.5	12.8	10M	1.32	64.3	
360	120	855	840	80	160	144	28.9	19.6	8M	1.27	32.5	
360	120	856	840	80	160	144	28.9	19.6	8M	1.27	31.0	
360	120	857	840	80	160	144	28.9	19.6	8M	1.27	41.0	
360	120	858	840	80	160	144	28.9	19.6	8M	1.27	36.0	
360	120	859	840	80	160	144	28.9	19.6	8M	1.27	18.0	
192	128	1122	707	38	58	0	29.4	14.7	12M	1.37	11.3	[21]
192	128	1122	707	45	67	0	29.4	14.7	12M	1.37	14.2	
192	128	1122	707	51	77	0	29.4	14.7	12M	1.37	15.6	
175	175	1081	483	40	100	0	29.4	13.7	14M	1.42	29.2	
132	198	1160	753	64	78	69	25.5	12.8	10M	1.32	50.3	
200	200	1074	716	9	56	145	29.5	11.5	10M	1.32	31.7	
200	200	1068	712	12	74	133	29.5	11.5	10M	1.32	49.3	
200	200	1062	708	15	93	122	29.5	11.5	10M	1.32	58.2	
200	200	1068	712	19	62	139	29.5	11.5	10M	1.32	44.4	
200	200	1056	704	12	124	104	29.5	11.5	10M	1.32	65.0	
200	200	1074	716	15	93	102	29.5	11.5	10M	1.32	65.7	
200	200	1050	700	15	93	102	29.5	11.5	10M	1.32	42.3	
200	200	1529	764	22	218	80	28.1	14.7	10M	1.32	11.3	[22]
200	200	1730	865	22	218	0	28.1	14.7	10M	1.32	34.6	
200	200	1660	830	22	218	33	28.1	14.7	10M	1.32	19.7	

200	200	1580	790	22	218	67	28.1	14.7	10M	1.32	9.7	
200	200	1554	777	22	218	73	28.1	14.7	10M	1.32	10.6	
300	200	805	925	50	125	12	29.4	14.7	12M	1.37	39.0	
136	203	1160	753	65	80	63	25.5	12.8	10M	1.32	50.3	
204	204	1113	635	24	48	175	29.4	14.7	8M	1.27	42.3	[23]
204	204	1113	635	24	48	175	29.4	14.7	8M	1.27	51.8	
204	204	1113	635	24	48	175	29.4	14.7	8M	1.27	51.3	
204	204	1113	635	24	48	175	29.4	14.7	8M	1.27	49.0	
205	205	1290	549	41	102	93	29.4	13.7	8M	1.27	37.0	[24]
205	205	1290	439	41	102	93	29.4	13.7	8M	1.27	39.0	
205	205	1290	329	41	102	93	29.4	13.7	8M	1.27	40.5	
205	205	1290	220	41	102	93	29.4	13.7	8M	1.27	26.9	
205	205	1290	549	41	102	55	29.4	13.7	8M	1.27	45.9	[25]
205	205	1290	439	41	102	55	29.4	13.7	8M	1.27	48.1	
205	205	1290	329	41	102	55	29.4	13.7	8M	1.27	51.1	
205	205	1290	220	41	102	55	29.4	13.7	8M	1.27	33.6	
205	205	1290	549	41	102	93	29.4	13.7	8M	1.27	45.9	[26]
205	205	1290	549	41	102	93	29.4	13.7	8M	1.27	48.1	
205	205	1290	549	41	102	93	29.4	13.7	8M	1.27	51.1	
205	205	1290	549	41	102	93	29.4	13.7	8M	1.27	33.6	
205	205	1293	554	41	102	55	29.4	13.7	10M	1.32	53.5	[27]
205	205	1293	554	41	102	90	29.4	13.7	10M	1.32	52.5	
205	205	1290	549	41	102	55	29.4	13.7	10M	1.32	53.5	[28]
205	205	1293	554	41	102	90	29.4	13.7	10M	1.32	70.4	[27]
205	205	1290	549	41	102	55	28.0	8.0	8M	1.27	38.3	[28]
205	205	1290	549	41	102	55	28.0	8.0	8M	1.27	40.5	
205	205	1290	549	41	102	55	28.0	8.0	8M	1.27	43.7	
205	205	1290	549	41	102	55	28.0	8.0	8M	1.27	46.2	
205	205	1290	549	41	102	55	28.0	8.0	8M	1.27	36.2	
205	205	1290	549	41	102	93	29.4	13.7	8M	1.27	45.9	[29]
205	205	1290	549	41	102	93	29.4	13.7	8M	1.27	48.1	
205	205	1290	549	41	102	93	29.4	13.7	8M	1.27	51.1	
205	205	1290	549	41	102	93	29.4	13.7	8M	1.27	33.6	
205	205	1290	549	41	102	55	29.4	13.7	8M	1.27	45.9	[25]
205	205	1290	549	41	102	55	29.4	13.7	8M	1.27	48.1	
205	205	1290	549	41	102	55	29.4	13.7	8M	1.27	51.1	
205	205	1290	549	41	102	55	29.4	13.7	8M	1.27	33.6	
205	205	1293	554	41	102	90	29.4	13.7	10M	1.32	52.5	[30]
205	205	1293	554	41	102	90	29.4	13.7	10M	1.32	54.1	
205	205	1293	554	41	102	90	29.4	13.7	10M	1.32	56.3	
205	205	1293	554	41	102	42	29.4	13.7	10M	1.32	56.5	[31]
139	209	1160	753	67	82	57	25.5	12.8	10M	1.32	50.3	
140	210	1196	644	11	134	65	25.7	8.5	10M	1.32	45.0	[32]
140	210	1196	644	11	134	65	25.7	8.5	10M	1.32	47.5	
140	210	1196	644	11	134	65	25.7	8.5	10M	1.32	48.5	
140	210	1196	644	11	134	65	25.7	8.5	10M	1.32	12.5	

140	210	1081	483	40	100	0	29.4	13.7	14M	1.42	36.9	
212	212	1059	635	23	47	163	16.5	33.0	10M	1.32	52.0	
212	212	1059	635	67	168	0	16.5	33.0	10M	1.32	52.0	
213	213	1127	628	11	73	123	32.8	14.7	10M	1.32	58.4	
213	213	1065	390	164	0	58	29.4	14.7	12M	1.37	34.0	
213	213	1065	390	82	82	67	29.4	14.7	12M	1.37	38.0	
213	213	1127	628	11	73	123	32.8	14.7	10M	1.32	59.2	
213	213	1127	628	11	73	123	32.8	14.7	10M	1.32	58.4	[33]
213	213	1135	617	10	65	136	32.8	14.7	10M	1.32	46.7	
142	213	1145	742	69	84	62	25.5	12.8	10M	1.32	50.3	
144	216	1145	742	69	85	59	25.5	12.8	10M	1.32	50.3	
145	218	1111	721	70	86	76	25.5	12.8	10M	1.32	50.3	
146	219	1145	742	70	86	56	25.5	12.8	10M	1.32	50.3	
225	225	1164	627	45	113	45	29.4	14.7	14M	1.42	44.1	[34]
225	225	1164	627	45	113	45	29.4	14.7	14M	1.42	41.1	[35]
225	225	1164	627	45	113	45	29.4	14.7	14M	1.42	42.7	
225	225	1164	627	45	113	45	29.4	14.7	14M	1.42	42.8	
225	225	1164	627	45	113	45	29.4	14.7	14M	1.42	43.7	
225	225	1164	627	45	113	45	29.4	14.7	14M	1.42	41.7	
225	225	1164	627	45	113	45	29.4	14.7	14M	1.42	41.9	
225	225	1164	627	45	113	45	29.4	14.7	14M	1.42	42.6	
225	225	1164	627	45	113	45	29.4	14.7	14M	1.42	46.0	
225	225	1164	627	45	113	45	29.4	14.7	14M	1.42	47.2	
225	225	1164	627	45	113	45	29.4	14.7	14M	1.42	46.3	
225	225	790	960	58	145	25	29.4	13.7	8M	1.27	40.4	[36]
225	225	791	960	58	145	25	29.4	13.7	10M	1.32	43.0	
225	225	792	960	58	145	25	29.4	13.7	12M	1.37	45.7	
225	225	790	960	58	145	25	29.4	13.7	8M	1.27	40.4	[36]
225	225	790	960	58	145	25	29.4	13.7	10M	1.32	43.0	
225	225	790	960	58	145	25	29.4	13.7	12M	1.37	45.7	
151	227	1111	721	73	89	66	25.5	12.8	10M	1.32	50.3	
153	230	1111	721	74	90	63	25.5	12.8	10M	1.32	50.3	
158	237	1277	547	52	129	0	29.4	14.7	8M	1.27	28.4	[37]
158	237	1277	547	52	129	0	29.4	14.7	4M	1.14	34.8	
158	237	1277	547	52	129	0	29.4	14.7	4M	1.14	37.2	
158	237	1277	547	52	129	0	29.4	14.7	4M	1.14	33.2	
159	239	1111	721	77	94	52	25.5	12.8	10M	1.32	50.3	
240	240	850	840	80	160	144	28.9	19.6	8M	1.27	34.0	
240	240	851	840	80	160	144	28.9	19.6	8M	1.27	33.0	
240	240	852	840	80	160	144	28.9	19.6	8M	1.27	41.5	
240	240	853	840	80	160	144	28.9	19.6	8M	1.27	37.0	
240	240	854	840	80	160	144	28.9	19.6	8M	1.27	19.0	
163	245	1294	554	41	103	0	28.0	8.0	8M	1.27	45.6	
105	245	1081	483	40	100	0	29.4	13.7	14M	1.42	35.7	
163	245	1294	554	41	103	0	34.8	16.5	10M	1.32	43.4	[38]
250	250	805	925	50	125	12	29.4	14.7	12M	1.37	42.3	

258	258	1176	505	59	147	0	25.0	7.5	10M	1.32	54.3	
67	267	1160	753	64	79	62	25.5	12.8	10M	1.32	31.7	
135	270	1000	850	57	143	0	29.4	13.7	12M	1.37	38.6	
68	274	1160	753	66	81	56	25.5	12.8	10M	1.32	31.7	
69	276	1145	742	67	81	64	25.5	12.8	10M	1.32	31.7	
120	280	1210	652	53	107	0	15.4	53.9	10M	1.32	56.5	
70	280	1081	483	40	100	0	29.4	13.7	14M	1.42	32.9	
70	281	1160	753	68	83	50	25.5	12.8	10M	1.32	31.7	
71	283	1145	742	68	83	58	25.5	12.8	10M	1.32	31.7	
122	286	1294	554	41	103	0	28.0	8.0	8M	1.27	42.5	
72	289	1160	753	70	85	43	25.5	12.8	10M	1.32	31.7	
73	291	1145	742	70	85	51	25.5	12.8	10M	1.32	31.7	
73	294	1111	721	71	86	69	25.5	12.8	10M	1.32	31.7	
150	300	1058	743	52	128	0	27.0	8.0	12M	1.37	35.4	
100	300	1207	650	53	107	0	15.4	53.9	10M	1.32	45.0	
100	300	1222	658	53	107	0	15.4	53.9	12M	1.37	57.0	
100	300	1246	671	47	93	0	15.4	53.9	10M	1.32	48.5	
100	300	1223	659	46	114	0	15.4	53.9	10M	1.32	45.0	
200	300	805	925	50	125	12	29.4	14.7	12M	1.37	40.2	
75	301	1111	721	73	89	62	25.5	12.8	10M	1.32	31.7	
102	307	1290	549	41	102	55	29.4	13.7	10M	1.32	35.4	
77	309	1111	721	75	91	55	25.5	12.8	10M	1.32	31.7	
35	315	1081	483	40	100	0	29.4	13.7	14M	1.42	29.5	[39]
79	318	1111	721	77	93	47	25.5	12.8	10M	1.32	31.7	[40]
106	319	1121	583	10	107	101	32.8	14.7	10M	1.32	56.8	
106	319	1121	583	10	107	101	32.8	14.7	10M	1.32	57.5	
106	319	1109	603	7	78	130	32.8	14.7	10M	1.32	29.5	
80	320	704	973	29	158	0	32.2	11.2	10M	1.32	42.9	[41]
80	320	1209	651	46	114	0	30.0	11.5	14M	1.42	47.0	
80	320	1209	651	64	96	0	30.0	11.5	14M	1.42	54.0	
80	320	1216	655	40	100	8	30.0	11.5	14M	1.42	35.0	
80	320	1216	655	56	84	8	30.0	11.5	14M	1.42	45.0	
80	320	1203	648	53	107	0	15.4	53.9	10M	1.32	42.5	
80	320	1203	648	53	107	0	15.4	53.9	12M	1.37	45.0	
80	320	1227	661	47	93	0	15.4	53.9	10M	1.32	42.5	
80	320	704	973	29	158	0	32.3	11.8	10M	1.32	44.6	[42]
80	320	704	973	29	158	0	32.2	11.2	10M	1.32	46.0	[43]
80	320	1216	655	100	40	8	30.0	11.5	14M	1.42	35.0	
82	326	1294	554	41	103	0	28.0	8.0	8M	1.27	34.3	
60	340	1209	651	46	114	0	30.0	11.5	14M	1.42	46.6	
60	340	1209	651	46	114	0	30.0	11.5	14M	1.42	46.6	
60	340	1200	646	53	107	0	15.4	53.9	10M	1.32	29.0	
60	340	1200	646	53	107	0	15.4	53.9	12M	1.37	36.0	
60	340	1209	651	47	93	0	15.4	53.9	10M	1.32	32.0	
60	340	1184	637	64	96	0	15.4	53.9	10M	1.32	30.0	
85	340	1065	390	164	0	58	29.4	14.7	12M	1.37	40.0	[44]

85	340	1065	390	82	82	67	29.4	14.7	12M	1.37	36.0	
80	340	1216	655	40	100	8	30.0	11.5	14M	1.42	34.7	
172	343	1031	724	52	128	0	27.0	8.0	12M	1.37	30.3	[45]
150	350	805	925	50	125	12	29.4	14.7	12M	1.37	38.8	
40	360	1209	651	46	114	0	30.0	11.5	14M	1.42	38.3	[46]
40	360	1218	656	40	100	6	30.0	11.5	14M	1.42	33.3	
40	360	1209	651	46	114	0	30.0	11.5	14M	1.42	38.3	[47]
40	360	1218	656	40	100	6	30.0	11.5	14M	1.42	33.3	
40	360	1209	651	46	114	0	30.0	11.5	14M	1.42	40.0	[48]
40	360	1209	651	64	96	0	30.0	11.5	14M	1.42	43.0	
40	360	1216	655	40	100	8	30.0	11.5	14M	1.42	27.0	
40	360	1216	655	56	84	8	30.0	11.5	14M	1.42	27.0	
40	360	1197	644	53	107	0	15.4	53.9	10M	1.32	22.0	[49]
40	360	1216	655	40	100	8	30.0	11.5	14M	1.42	27.0	[50]
90	360	1000	850	57	143	0	29.4	13.7	12M	1.37	36.3	
120	360	845	840	80	160	144	28.9	19.6	8M	1.27	40.0	
120	360	846	840	80	160	144	28.9	19.6	8M	1.27	37.0	
120	360	847	840	80	160	144	28.9	19.6	8M	1.27	48.0	
120	360	848	840	80	160	144	28.9	19.6	8M	1.27	31.0	
120	360	849	840	80	160	144	28.9	19.6	8M	1.27	21.0	
40	360	1216	655	100	40	8	30.0	11.5	14M	1.42	27.0	[51]
40	360	1216	655	100	40	8	30.0	11.5	14M	1.42	27.0	
41	367	1294	554	41	103	0	28.0	8.0	8M	1.27	21.1	[52]
165	385	913	508	97	244	0	29.4	14.7	12M	1.37	43.3	[53]
100	400	805	925	50	125	12	29.4	14.7	12M	1.37	34.9	
45	405	1000	850	57	143	0	29.4	13.7	12M	1.37	35.9	[54]
50	450	805	925	50	125	12	29.4	14.7	12M	1.37	31.3	[55]

1 MPa = 0.145 ksi

Table 2 – Statistics of the raw experimental data

Variable	Minimum	Maximum	Average	[a]SD	Skewness	Kurtosis
Fly ash/Slag ratio	0.25	5.67	1.636338	1.265632	1.329057	0.661458
Water/Solid ratio	0.269	0.925	0.319204	0.093986	0.092207	-1.04618
Activator/Binder ratio	0.269	0.925	0.393491	0.065017	-0.56924	1.763769
Na_2SiO_3/NaOH ratio	1	8.769	2.076436	0.554776	-0.83189	-1.02217
NaOH molarity	8	16	10.07746	2.297312	0.21715	-0.2579
Compressive strength (MPa)	20	89	42.84886	11.0641	-0.02721	0.270916

[a]Standard Deviation; 1 MPa = 0.145 ksi

Table 3 – Model performance metrics

	R^2	RMSE (MPa)	MAE (MPa)
ANN	0.86331	5.61	3.77
MARS	0.83835	6.01	4.14

1 MPa = 0.145 ksi

Table 4 – Mix design of slag–fly ash blended concrete (kg/m^3)

Mix Notation	Target Strength	Mix design variables obtained from Contours (Fig. 8)				
		Water/Solid	Activator/Binder	Na_2SiO_3/NaOH	NaOH molarity	Fly ash/Slag
M25	25 MPa	0.40	0.65	4.2	9.0	6.5
M30	30 MPa	0.33	0.70	3.2	10.5	6.0
M40	40 MPa	0.30	0.54	2.2	11.5	3.0
M45	45 MPa	0.40	0.40	4.0	12.0	1.0

Mix Notation	Target Strength	Calculated Mix Proportions (kg/m^3)						
		Fly ash	Slag	Sand	Aggregates	Na_2SiO_3	NaOH	Added water
M25	25 MPa	355.3	54.7	518.3	1001.0	215.3	51.3	50.50
M30	30 MPa	351.4	58.6	545.9	1054.4	218.7	68.3	5.40
M40	40 MPa	307.5	102.5	575.0	1110.6	152.2	69.2	19.63
M45	45 MPa	205	205	565.6	1092.5	131.2	32.8	97.22

1 MPa = 0.145 ksi

Table 5 – Chemical composition of fly ash and slag

Fly ash	Component (wt. %)											
	SiO_2	Al_2O_3	Fe_2O_3	CaO	P_2O_5	TiO_2	MgO	K_2O	SO_3	MnO	Na_2O	LOI[a]
Fly ash	47.9	28.0	14.1	3.8	1.8	2.0	0.9	0.6	0.3	0.2	0.4	0.4
Slag	36.9	14.2	0.3	36.0	0.4	0.6	5.1	0.1	6.1	0.4	0	0.3

[a]Loss on ignition (unburnt carbon content)

Table 6 – Physical and mineralogical properties of fly ash and slag

Properties investigated		Fly ash	Slag
Specific Gravity		2.25	2.95
BET Surface Area, (m^2/kg)		2363	3582
	at 10 microns	43.1	43.5
Fineness (%)	at 20 microns	61.9	71.9
	at 45 microns	82.7	96.9
Amorphous content (%)		71.8	71.7
Crystalline content (%)		27.8	28.0

1 m^2/kg = 704.5 in^2/lb

FIGURES

List of Figures

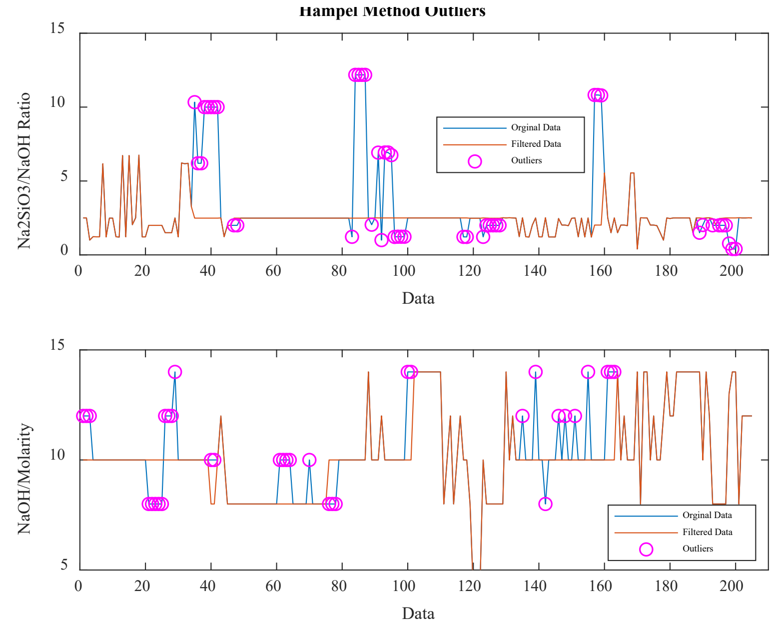
Hampel Method Outliers
Na2SiO3/NaOH Ratio
Data
Orginal Data
Filtered Data
Outliers
NaOH/Molarity
Data
Orginal Data
Filtered Data
Outliers

Fig. 1

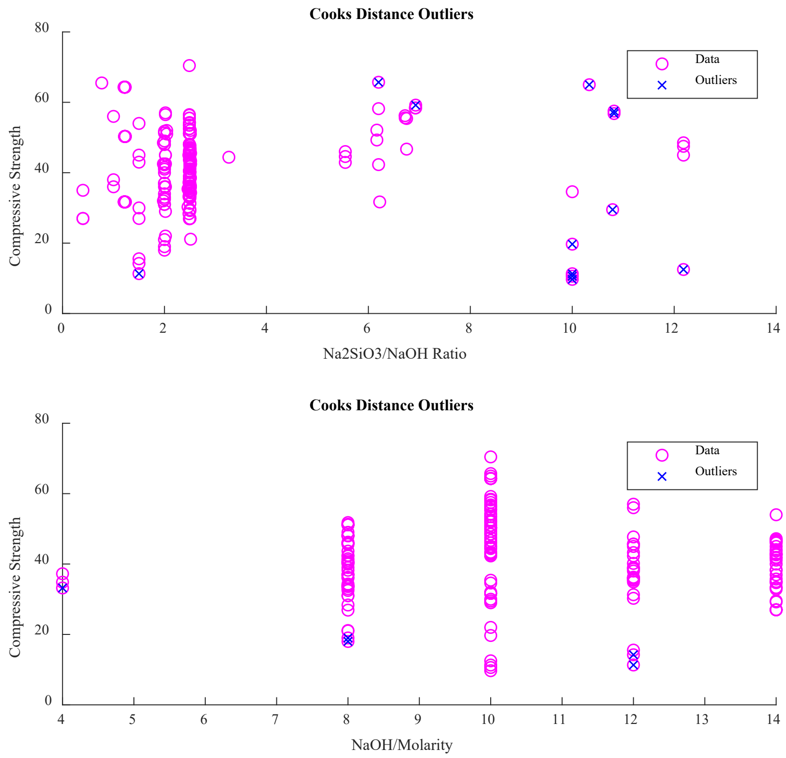
Cooks Distance Outliers
Compressive Strength
Na2SiO3/NaOH Ratio
Data
Outliers
Cooks Distance Outliers
Compressive Strength
NaOH/Molarity
Data
Outliers

Fig. 2

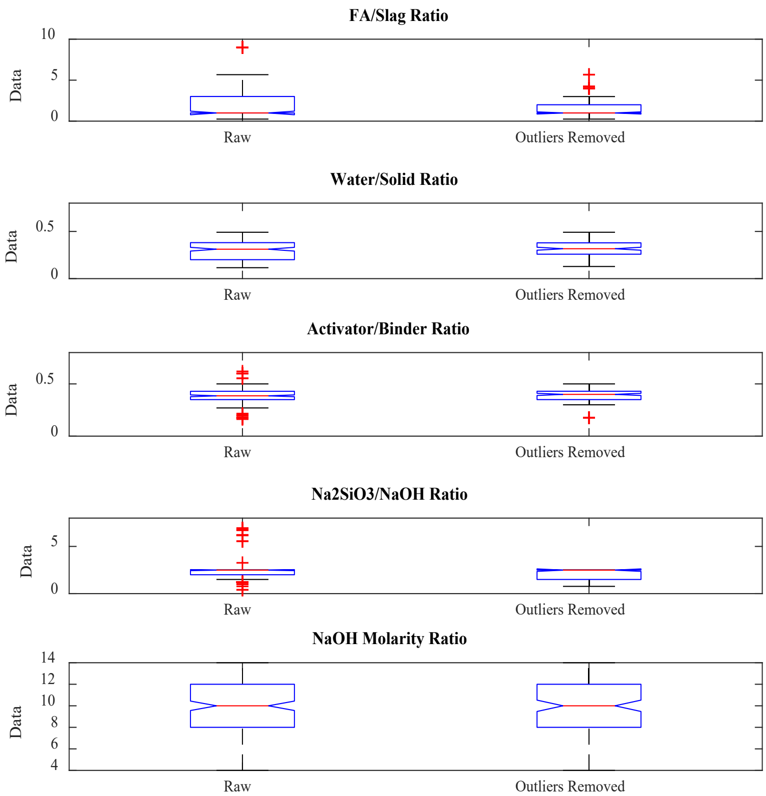
FA/Slag Ratio
Water/Solid Ratio
Activator/Binder Ratio
Na2SiO3/NaOH Ratio
NaOH Molarity Ratio
Data
Raw
Outliers Removed

Fig. 3

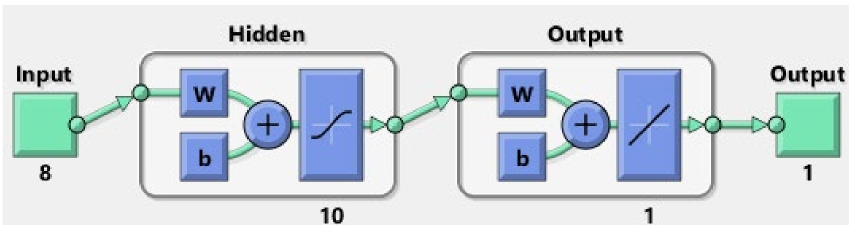
Input
8
Hidden
W
b
10
Output
W
b
1
Output
1

Fig. 4

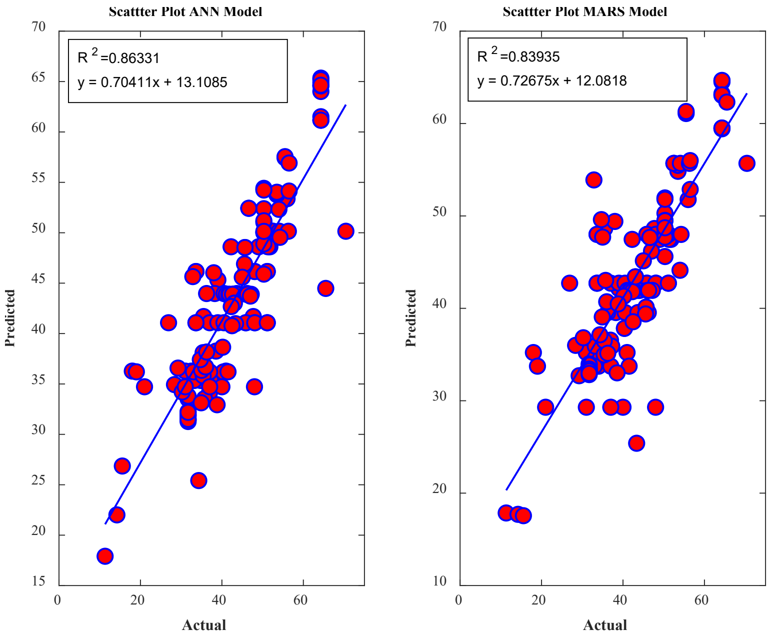
Scattter Plot ANN Model
R^2=0.86331
y = 0.70411x + 13.1085
Predicted
Actual
Scattter Plot MARS Model
R^2=0.83935
y = 0.72675x + 12.0818
Predicted
Actual

Fig. 5

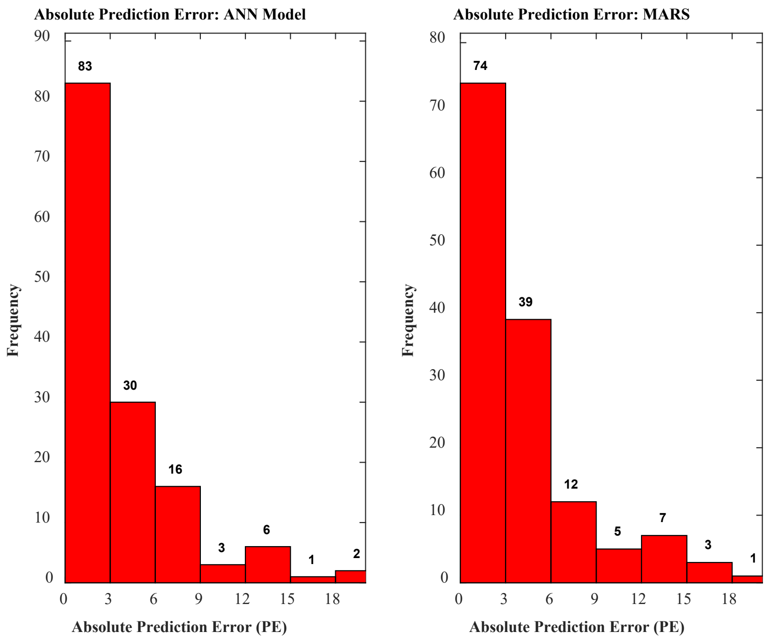
Absolute Prediction Error: ANN Model
Frequency
Absolute Prediction Error (PE)
83
30
16
3
6
1
2
Absolute Prediction Error: MARS
Frequency
Absolute Prediction Error (PE)
74
39
12
5
7
3
1

Fig. 6

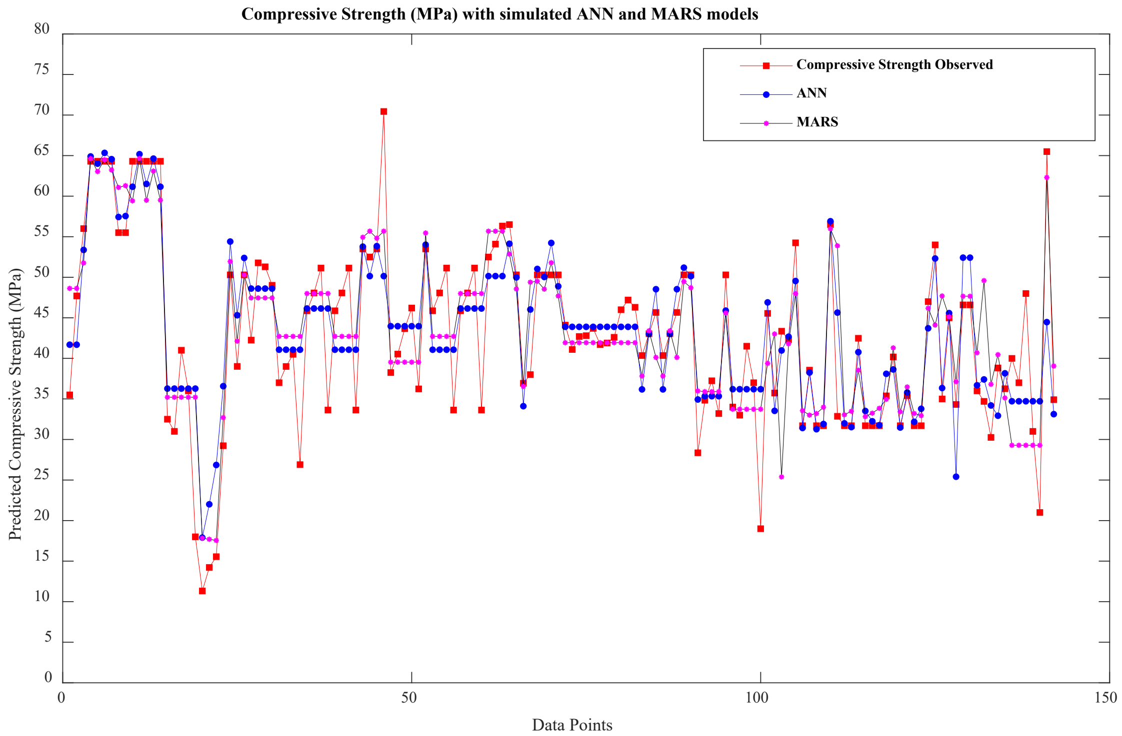

Fig. 7

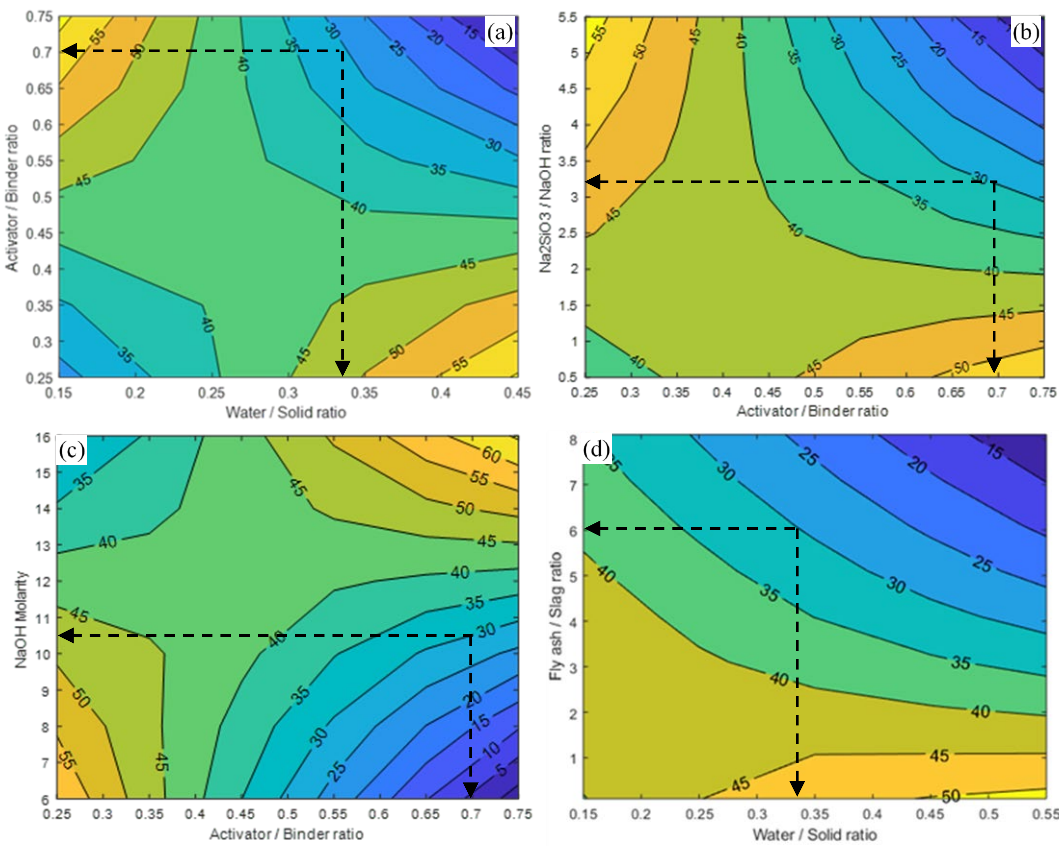

Note: M3O mix parameters are shown in dotted lines

Fig. 8

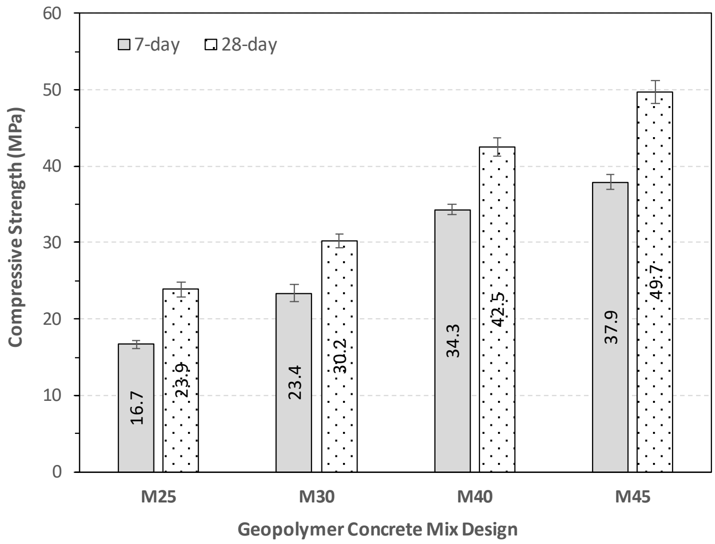
7-day
28-day
Compressive Strength (MPa)
0
10
20
30
40
50
60
16.7
23.9
23.4
30.2
34.3
42.5
37.9
49.7
M25
M30
M40
M45
Geopolymer Concrete Mix Design

Fig. 9